Journal of Controlled Release 337 (2021) 521–529

Contents lists available at ScienceDirect

Journal of Controlled Release

journal homepage: www.elsevier.com/locate/jconrel

Selective transferrin coating as a facile strategy to fabricate BBB-permeable and targeted vesicles for potent RNAi therapy of brain metastatic breast cancer *in vivo*

Yaohua Wei [a,b,1], Yinping Sun [a,1], Jingjing Wei [a], Xinyun Qiu [a], Fenghua Meng [a,*], Gert Storm [b,c,d,**], Zhiyuan Zhong [a,*]

[a] Biomedical Polymers Laboratory, College of Chemistry, Chemical Engineering and Materials Science, State Key Laboratory of Radiation Medicine and Protection, Soochow University, Suzhou 215123, PR China
[b] Department of Biomaterials Science and Technology, MIRA Institute for Biological Technology and Technical Medicine, University of Twente, PO Box 217, 7500AE Enschede, the Netherlands
[c] Department of Pharmaceutics, Utrecht University, the Netherlands
[d] Department of Surgery, Yong Loo Lin School of Medicine, National University of Singapore, Kent Ridge, Singapore

ARTICLE INFO

Keywords:
Transferrin
Polymersomes
Brain metastases
RNAi
Targeted delivery

ABSTRACT

Brain metastases are a most disturbing situation for breast cancer patients as there is basically no adequate treatment available. Any potential drug formulation has to be able to cross the blood-brain barrier (BBB) and specific to metastatic brain tumors without causing unacceptable adverse effects. Here, we developed transferrin-functionalized chimeric polymersomes carrying siRNA against polo-like kinase 1 (Tf@TBP-CPs-siPLK1) for treating brain metastatic MDA-MB 231 triple negative breast cancer (TNBC) xenografts in mice. To facilitate the loading of siPLK1, chimaeric polymersomes (CPs) were designed with spermine in the watery core and transferrin-binding peptide (TBP) at the surface, enabling attachment of transferrin after the siRNA loading step and thereby circumventing interference of transferrin with siRNA loading. Tf@TBP-CPs-siPLK1 encapsulating 3.8 wt% siRNA had a mean size of about 50 nm and a neutral zeta potential in phosphate buffer (PB). By virtue of the presence of transferrin, Tf@TBP-CPs demonstrated greatly (*ca.* 5-fold) enhanced internalization in MDA-MB 231 cells and transcytosis in the endothelial (bEnd.3) monolayer model *in vitro* as well as markedly improved accumulation in the orthotopically xenografted MDA-MB 231 tumor in the brain *in vivo* compared with control CPs lacking transferrin, supporting that transferrin mediates efficient BBB penetration and high specificity towards MDA-MB 231 cells. As a result, Tf@TBP-CPs-siPLK1 effectively inhibited tumor progression and prolonged the lifespan of the mice significantly. Selective transferrin coating appears to be a particularly facile strategy to fabricate BBB-permeable and targeted vesicles for potent RNAi therapy of brain metastatic breast cancer.

1. Introduction

Brain metastases when occurring in cancerous patients with *e.g.* lung tumor, breast tumor, and melanoma are a most disturbing situation [1–3]. In breast cancer, human epidermal growth factor receptor 2 (HER-2) positive patients and triple-negative breast cancer (TNBC) patients have exhibited a particularly high risk to develop brain metastases [4,5]. To date, there is basically no treatment available for brain metastases because few drugs are capable of penetrating the blood-brain barrier (BBB) [6]. The median survival of breast cancer patients after diagnosis with brain metastases was only 7 months, in which further poor outcome was found for TNBC than HER-2 positive patients [7]. In recent years, different approaches have been explored to improve the treatment of breast cancer brain metastases [8,9]. For example, focused ultrasound was applied to disrupt the BBB and thereby to enhance the delivery of antibodies, antibody-drug conjugates, and nanomedicines to

* Corresponding authors.
** Corresponding author at: Department of Biomaterials Science and Technology, MIRA Institute for Biological Technology and Technical Medicine, University of Twente, PO Box 217, 7500AE Enschede, the Netherlands.
E-mail addresses: fhmeng@suda.edu.cn (F. Meng), G.Storm@uu.nl (G. Storm), zyzhong@suda.edu.cn (Z. Zhong).
[1] Y.H. Wei and Y.P. Sun contribute equally to this work.

https://doi.org/10.1016/j.jconrel.2021.07.048
Received 19 January 2021; Received in revised form 31 May 2021; Accepted 30 July 2021
Available online 2 August 2021

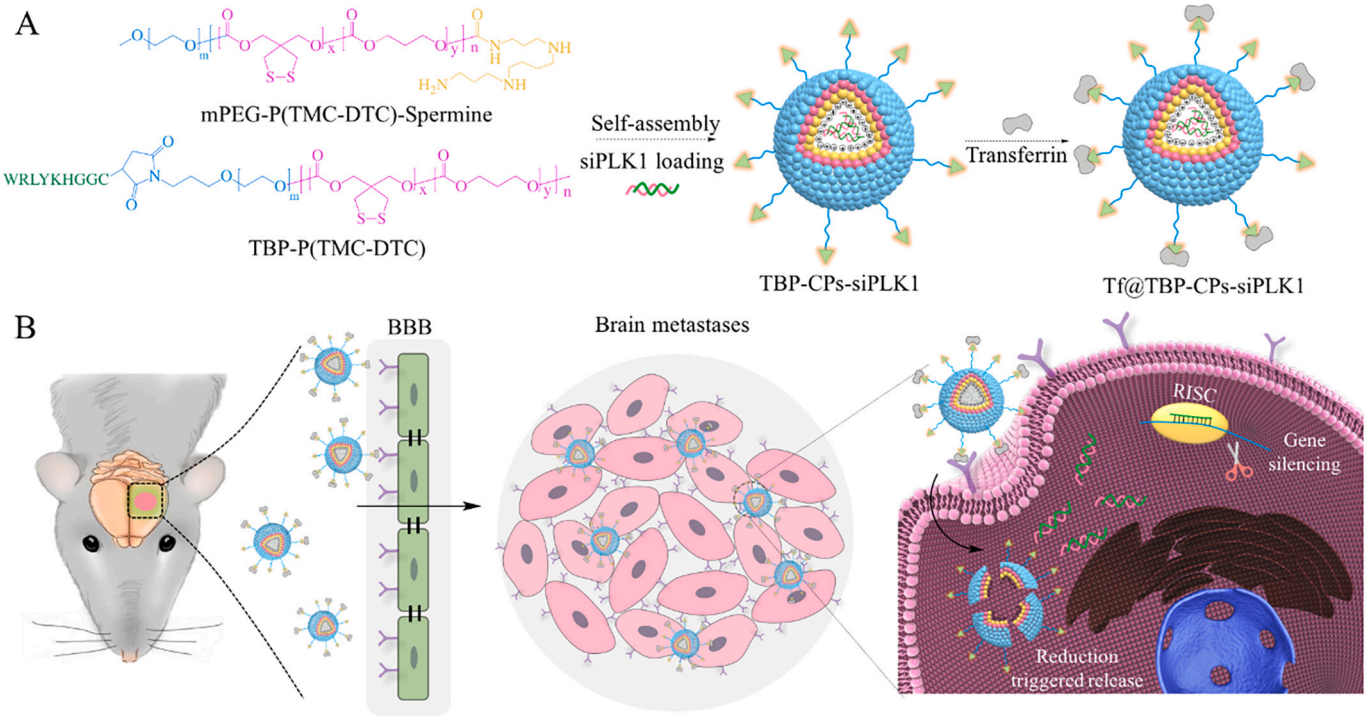

Scheme 1. Illustration of the fabrication of Tf functionalized polymersomal siPLK1 (Tf@TBP-CPs-siPLK1) (A), and the targeted delivery of siPLK1 to brain metastases *in vivo* (B).

brain metastases [10]. Ligand mediated, BBB-permeable nanosystems that employ low density lipoprotein receptor related protein 1 (LRP1) pathway alone or in combination with receptor targeting antibody were investigated for improved treatment of brain metastatic breast cancers [11–13]. Intravenously administered cell-penetrating peptide-functionalized nanomedicines containing doxorubicin and intracranial delivery of plasmid encoding trastuzumab were also reported to suppress the growth of brain metastases [14,15]. Notably, most previous receptor-mediated transcytosis (RMT) systems deal with the use of highly toxic drugs, which would most probably also cause serious adverse effects, given the fact that a large part of the administered dose is distributed to other locations in the body than the target [16].

Different from many chemotherapeutic anticancer drugs, small interfering RNA (siRNA) with a specific target in cancer cells possesses usually low off-target toxicity [17]. A number of siRNA drugs have been studied for treating distinct tumors [18,19]. siRNA silencing Polo-like kinase 1 (siPLK1), a highly conserved serine-threonine kinase that is overexpressed in diverse cancer types and correlated with poor prognosis [20], has shown to be able to suppress growth of various tumors including lung and breast tumors *in vivo* [21,22]. The clinical application of siRNA is, however, limited by *in vivo* delivery hurdles like poor tumor cell uptake, rapid degradation by nucleases, and poor endosomal escape [18,23]. Therefore, the development of efficient delivery vehicles is a challenging task in siRNA applications [24,25]. In case of brain metastases, the vehicles need to carry siRNA across the BBB. Transferrin is one of the few ligands that have been reported to be capable of penetrating the BBB *via* transferrin receptor (TfR)-mediated transcytosis (RMT) [26–32]. TfR is also overexpressed by a range of malignant tumor cells including those of glioblastoma and breast tumors [33,34]. Transferrin-drug conjugates and transferrin-functionalized nanomedicines have been explored for glioblastoma and breast tumor RNAi therapy [35,36]. There are also reports on transferrin-directed siRNA nanocaplet for targeted RNA interference and deep tumor penetration, which generally require dedicated fabrication [37].

Here, we report on facile fabrication of BBB-permeable and targeted vesicles *via* selective transferrin coating strategy for potent RNAi therapy of brain metastatic breast cancer *in vivo*. Transferrin-functionalized chimeric polymersomes carrying siPLK1 (Tf@TBP-CPs-siPLK1) were simply obtained by treating siPLK1-loaded transferrin binding peptide exposing chimeric polymersomes (TBP-CPs-siPLK1) with transferrin, thus circumventing interference of surface-bound transferrin with siRNA loading (Scheme 1). TBP (sequence: CGGGHKYLRW) was reported to specifically bind to transferrin [38]. We have previously shown that transferrin-bound polymersomal doxorubicin hydrochloride prepared by TBP-exposing CPs exhibited transferrin-induced enhanced cellular uptake and antitumor efficacy in a subcutaneous colorectal cancer model [39]. Based on the literature, as cited above, it was hypothesized that Tf@TBP-CPs-siPLK1 would not only cross BBB but also target to brain metastatic TfR-overexpressed TNBC cells, resulting in potent and low toxic RNAi therapy for malignant breast tumor brain metastases.

2. Experimental section

2.1. Materials

siPLK1 (SS: 5′-AGAUCACCCUCCUUAAAUAUU-3′, AS: 5′-UAUUUAAGGAGGGUGAUCUUU-3′), Cy3 or Cy5-labeled siPLK1 (siPLK1(Cy3), siPLK1(Cy5)), siEGFP (SS 5’-GACGUAAACGGCCACAAGUdTdC-3′, AS: 5’-ACUUGUGGCCGUUUACGUCdGdC-3′), and siScramble (SS: 5’-UUCUCCGAACGUGUCACGUTT-3′, AS: 5’-ACGUGACACGUUCGGAGAATT-3′) were obtained from Gene Pharma (China).

2.2. Preparation of Tf@TBP-CPs-siRNA

Poly(ethylene glycol)-*b*-poly(trimethylene carbonate-co-dithiolane trimethylene carbonate)-spermine (PEG-P(TMC-DTC)-sp, M_n = 5.0-(15.0–2.0)-0.2 kg/mol) copolymer was synthesized as previously reported [40]. TBP-PEG-P(TMC-DTC) was synthesized *via* Michael addition between TBP and MAL-PEG-P(TMC-DTC) [39]. siRNA (siPLK1, siEGFP or siScramble) loaded Tf@TBP-CPs were obtained *via* solvent

exchange method. Typically, PEG-P(TMC-DTC)-sp and TBP-PEG-P (TMC-DTC) at weight ratio of 80/20 were dissolved in DMSO at 5 mg/mL. The polymer solution was then added into 900 μL HEPES (5 mM, pH 6.8) containing siRNA and incubated for 2 h without stirring and at 25 °C overnight in an incubator at 100 rpm to allow the formation of TBP-CPs-siPLK1. TBP-CPs-siPLK1 was purified by dialysis (MWCO 350 kDa) in PB (10 mM, pH 7.4) for 6 h. The siRNA loading efficiency was quantified by NanoDrop 2000c spectrophotometer at 260 nm. Tf@TBP-CPs-siPLK1 was attained by adding Tf solution into TBP-CPs-siPLK1. Briefly, TBP-CPs-siPLK1 with TBP surface density of 17.2% (2 mg/mL, 1 mL) was incubated with 2.7 μM Tf (TBP/Tf = 1/1, mol/mol). BCA assays were used to determine the Tf surface densities. The size and zeta potential of Tf@TBP-CPs-siPLK1 before and after Tf coating were tested.

2.3. Investigation of endocytotic pathway of Tf@TBP-CPs-siPLK1

MDA-MB 231 cells (2×10^5 cells/well) were seeded in 6-well plates and cultured for 24 h prior to adding Tf@TBP-CPs-siPLK1(Cy5) (1 μg siRNA/mL). To investigate the energy-dependent process, cells were co-incubated with Tf@TBP-CPs-siPLK1(Cy5) at 4 °C or in the presence of NaN_3 (10 mM) at 37 °C for 1 h. The cells were washed, harvested and re-suspended in 500 μL PBS for flow cytometry analysis by BD FACS Calibur flow cytometer (Becton Dickinson, USA) based on 10,000 gated events. The endocytic pathway was further investigated by adding inhibitors including chlorpromazine (10 μg/mL), amiloride hydrochloride (1 mg/mL) and β-CD (1 mg/mL) to incubate for 1 h at 37 °C prior to addition of Tf@TBP-CPs-siPLK1(Cy5). After 1 h, the cells were similarly treated immediately before flow cytometry analysis. The cells treated with CPs-siPLK1(Cy5) at 37 °C were used as control.

2.4. Intracellular siPLK1 delivery and in vitro gene silencing

MDA-MB 231 cells were seeded in 6-well plates (5×10^5 cells/well) and cultured for 24 h. CPs-siPLK1(Cy5) and Tf@TBP-CPs-siPLK1(Cy5) were added and incubated for 4 h (1 μg siRNA /mL) and the cells were washed, harvested and re-suspended in 500 μL PBS for flow cytometry analyses. For each sample, 10,000 events were collected and MDA-MB 231 cells without any treatment were used as control. The *in vitro* cellular association of Tf@TBP-CPs-siPLK1(Cy5) with B-ALL-697 and MDA-MB-231 cells at 4 h post-incubation was investigated. MDA-MB 231 and B-ALL-697 cells were seeded in 12-well plates (2×10^5 cells/well) and cultured for 24 h prior to adding Tf@TBP-CPs-siPLK1 (Cy5) (100 nM siPLK1). After 4 h, the medium was decanted and the cells were washed (PBS, ×2) and collected for flow cytometry analysis.

The cellular uptake and intracellular siPLK1(Cy3) delivery were monitored *via* confocal laser scanning microscopy (CLSM) (Leica TCS SP5). Briefly, MDA-MB 231 cells were seeded on glass coverslips in 24-well plates (5×10^4 cells/well) and cultured for 24 h at 37 °C. Tf@TBP-CPs-siPLK1(Cy3) was added and incubated for 12 h at 37 °C (siPLK1 (Cy3): 5 μg/mL). The cells were then washed and fixed with 4% paraformaldehyde for 15 mins. After fixation, the nuclei were stained with DAPI (5 μg/mL) for 5 mins, washed, and finally examined with CLSM using a 63-x oil immersion objective. CPs-siPLK1(Cy3) was used as control.

The gene silencing capacity of siRNA (siEGFP) loaded Tf@TBP-CPs *in vitro* was investigated using MDA-MB 231-EGFP cells. In brief, the cells (5×10^3 cells/well) were cultured in 96-well plates for 24 h, and 10 μL of Tf@TBP-CPs-siEGFP or CPs-siEGFP was added (siRNA: 100 nM) and the cells without treatment were used as control ($n = 3$). After incubation for 12 h, the culture medium was replaced with 90 μL fresh medium, and the cells were further cultured for 36 h before the observation using fluorescence microscopy (Olympus BX41). The gene silencing efficacy of Tf@TBP-CPs-siEGFP and CPs-siEGFP was calculated by ImageJ in comparison to PBS treated group.

Table 1
Characterization of CPs-siPLK1, TBP-CPs-siPLK1 and Tf@TBP-CPs-siPLK1.

Entry	Formulation	Size (nm)[a]	PDI[a]	DLC (wt%)[b]	DLE (%)[b]	ζ (mV)[c]
1	CPs-siPLK1	52 ± 3	0.12	4.0 ± 0.1	83 ± 3	+ 0.1
2	TBP-CPs-siPLK1	50 ± 1	0.10	4.1 ± 0.1	85 ± 2	+ 0.4
3	Tf@TBP-CPs-siPLK1	53 ± 3	0.14	3.8 ± 0.1	80 ± 3	+ 0.2

[a] Determined by dynamic light scattering (DLS) in 5 mM PB (pH 7.4). The data are presented as mean ± standard deviation (SD) ($n = 3$).
[b] Determined by Nanodrop 2000c UV–Vis spectrophotometer at 260 nm. The data are presented as mean ± SD (n = 3).
[c] Determined by a zeta potential analyzer in 5 mM PB (pH 7.4).

2.5. MTT assays of Tf@TBP-CPs-siPLK1

MDA-MB 231cells were seeded in 96-well plates (3×10^3 cells/well) and after 24 h 20 μL of Tf@TBP-CPs-siPLK1 was added. Following 12 incubation, the medium was replaced with fresh medium, and the cells were further cultured 36 h. Then MTT solution (5 mg/mL) was added and incubated for 4 h at 37 °C. After removal of the medium, 150 μL DMSO was added to the cells. The absorbance at 492 nm was measured using a microplate reader (Multiskan FC), and the cell viability was expressed as the percentages of the absorbance of the cells treated with different formulations to that of PBS group ($n = 5$).

2.6. In vivo treatment of intracranial MDA-MB 231 metastases model

Mice were handled according to the protocols approved by Soochow University Laboratory Animal Center and the Animal Care and Use Committee of Soochow University. Intracranial MDA-MB 231 brain metastases model was established using female Balb/c nude mice *via* implantation of minced breast tumor tissue into the left stratum of the mice, and this day was designated as day 0. On day 10, the mice were imaged and divided into 4 groups ($n = 9$) before the intravenous injection of Tf@TBP-CPs-siPLK1, CPs-siPLK1, Tf@TBP-CPs-siScrambe (2 mg siRNA/kg) or PBS *via* tail veins on day 10, 12, 14, and 16. The tumor development was tracked on day 13, 16 and 19 using an Lumina IVIS II *in vivo* imaging system. The mice were weighed every two days and the weight was normalized to their initial values. The survival curves of the mice were recorded. On day 20, one mouse of each group was selected and perfused with Evans Blue before sacrifice and excision of major organs and brain tumors for hematoxylin and eosin (H&E) staining and observation with a digital microscope.

2.7. Statistical analyses

One-way analysis of variance (ANOVA) with Tukey multiple comparison test (Prism) was used to determine the significance among groups. Statistical significance was established at $^*p < 0.05$, $^{**}p < 0.01$ and $^{***}p < 0.001$.

3. Results and discussion

3.1. Formation and characterization of Tf@TBP-CPs-siPLK1

Tf@TBP-CPs-siPLK1 were obtained by co-assembly of PEG-P(TMC-DTC)-sp and TBP-PEG-P(TMC-DTC) at a weight ratio of 80/20 in the presence of siPLK1, followed by binding Tf with these preformed polymersomes (Scheme 1). The TBP density at the particle surface was set at 17.2 mol% because that density showed optimal Tf binding and targeting effect to TfR-positive cancer cells earlier [39]. Table 1 shows that TBP-CPs-siPLK1 obtained at an initial start amount of siPLK1 of 5 wt% had an encapsulation efficiency of 85% and siPLK1 loading content of 4.1 wt%. The high siRNA encapsulation efficiency might be due to the electrostatic and hydrogen bonding interactions between siRNA

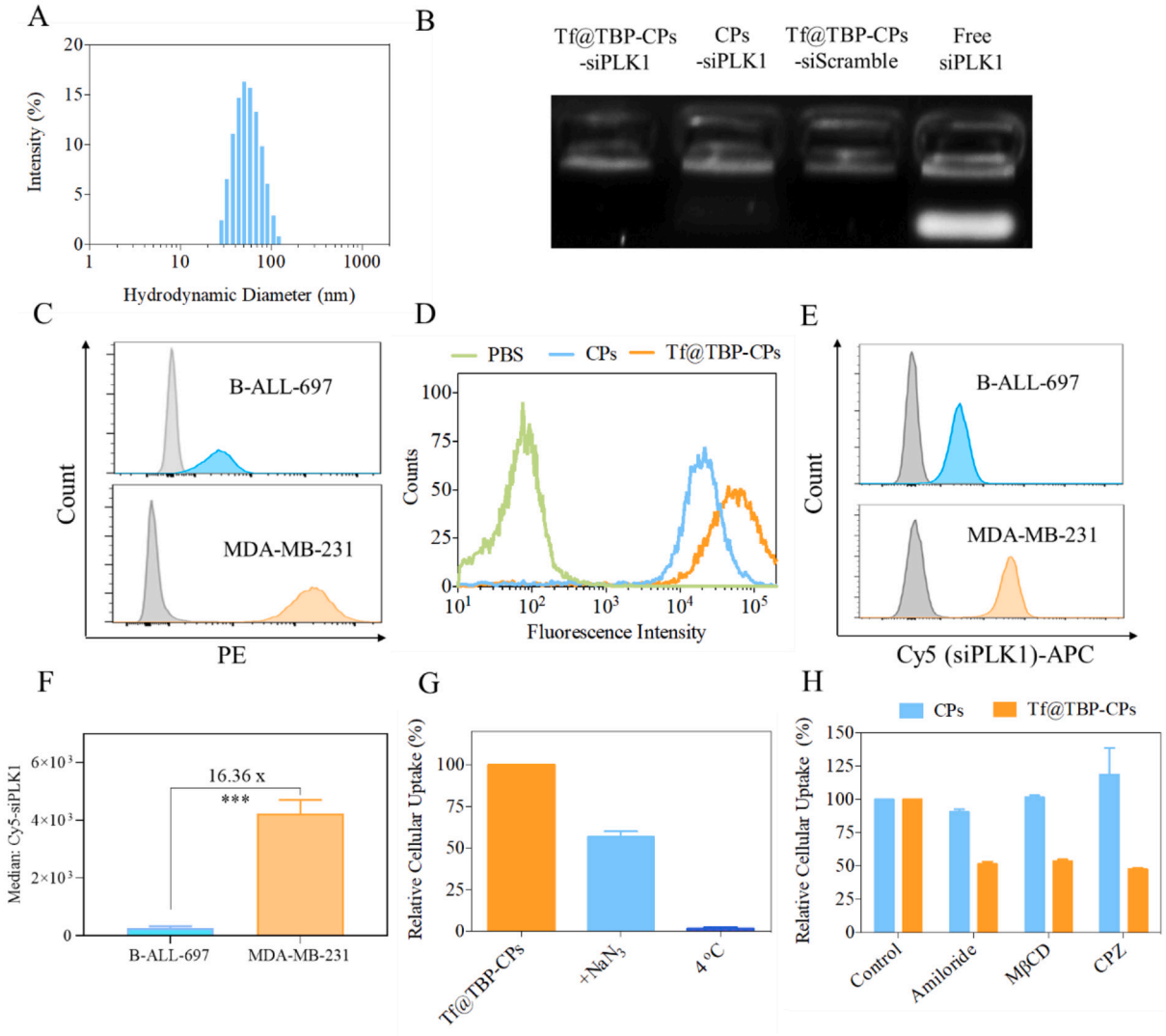

Fig. 1. (A) The size distribution of Tf@TBP-CPs-siPLK1 determined by DLS. (B) Gel electrophoresis of Tf@TBP-CPs-siPLK1, CPs-siPLK1,Tf@TBP-CPs-siSramble and free siPLK1. (C) TfR expression assays of MDA-MB 231 and B-ALL-697 cells. (D) The association of Tf@TBP-CPs-siPLK1(Cy5) and CPs-siPLK1(Cy5) following 4 h incubation with MDA-MB 231 cells as determined by flow cytometry. The *in vitro* cellular association (E) and semi-quantitative analysis (F) of Tf@TBP-CPs-siPLK1 (Cy5) with B-ALL-697 and MDA-MB-231 cells at 4 h post-incubation. (G) The relative cellular uptake of Tf@TBP-CPs-siPLK1(Cy5) in the presence of ATP inhibitor or at 4 °C. (H) The relative cellular uptake of CPs-siPLK1(Cy5) and Tf@TBP-CPs-siPLK1(Cy5) in the presence of various internalization inhibitors. The relative cellular uptake values were normalized to CPs-siPLK1(Cy5) and Tf@TBP-CPs-siPLK1(Cy5) without any pretreatment, respectively ($n = 3$).

(negatively charged) and spermine (positively charged) in the interior of the polymersomes and presence of robust polymersome membrane that prevents the leakage of siRNA [22]. Interestingly, TBP-CPs-siPLK exhibited a small mean size around 50 nm, narrow distribution with mean PDI of 0.10, and neutral zeta potential in the PB (pH 7.4). The incubation of preformed TBP-CPs-siPLK1 was performed with 2.7 μM Tf, which corresponded to a molar ratio of TBP/Tf = 1/1, yielded Tf@TBP-CPs-siPLK1 maintaining similar size distribution, siPLK1 loading and zeta potential (Table 1). Fig. 1A gives a representative hydrodynamic size distribution of Tf@TBP-CPs-siPLK1 as determined by DLS. The little influence of Tf binding on the degree of siPLK1 loading corroborates that siPLK1 is encapsulated in the core of polymersomes. The gel retardation assays confirmed complete and stable encapsulation of siRNA in the polymersomes (Fig. 1B). Previously we showed that the chimeric polymersomes based on PEG-P(TMC-DTC)-sp efficiently encapsulated protein drugs in the aqueous core and mediated efficient protein delivery *in vitro* and *in vivo* [41]. To assess the Tf coating stability on the TBP-CPs, Tf was labeled with radioactive ^{125}I and coated on freshly prepared TBP-Ps. The gamma counter results displayed that over 85% ^{125}I-Tf was kept on the surface of TBP-CPs after storage in PBS for 48 h, in the presence of 50-fold excess Tf, mouse whole blood or human serum, indicating that Tf is tightly bound and will not easily be exchanged by excessive Tf or other proteins in the blood [39]. The non-targeted CPs-siPLK1 were formulated with similar siRNA loading, size distribution, and zeta potential (Table 1).

3.2. TfR targeting and endocytosis pathways

The immunoassays showed that MDA-MB 231 cells had a high expression of TfR while B-ALL-697 cells were basically TfR-negative (Fig. 1C). The targetability and uptake of Tf@TBP-CPs-siPLK1 in MDA-MB 231 breast tumor cells was investigated using Cy5-labeled siPLK1 (siPLK1(Cy5)) as a model by flow cytometry. The results displayed that the presence of Tf on the surface of the CPs enhanced their cellular association, which was about 3-fold better than non-targeted CPs-siPLK1(Cy5) (Fig. 1D). Moreover, TfR-negative B-ALL-697 cells showed *ca.* 16-fold lower internalization of Tf@TBP-CPs than MDA-MB 231 cells (Fig. 1E, F), verifying the selectivity of Tf@TBP-CPs towards

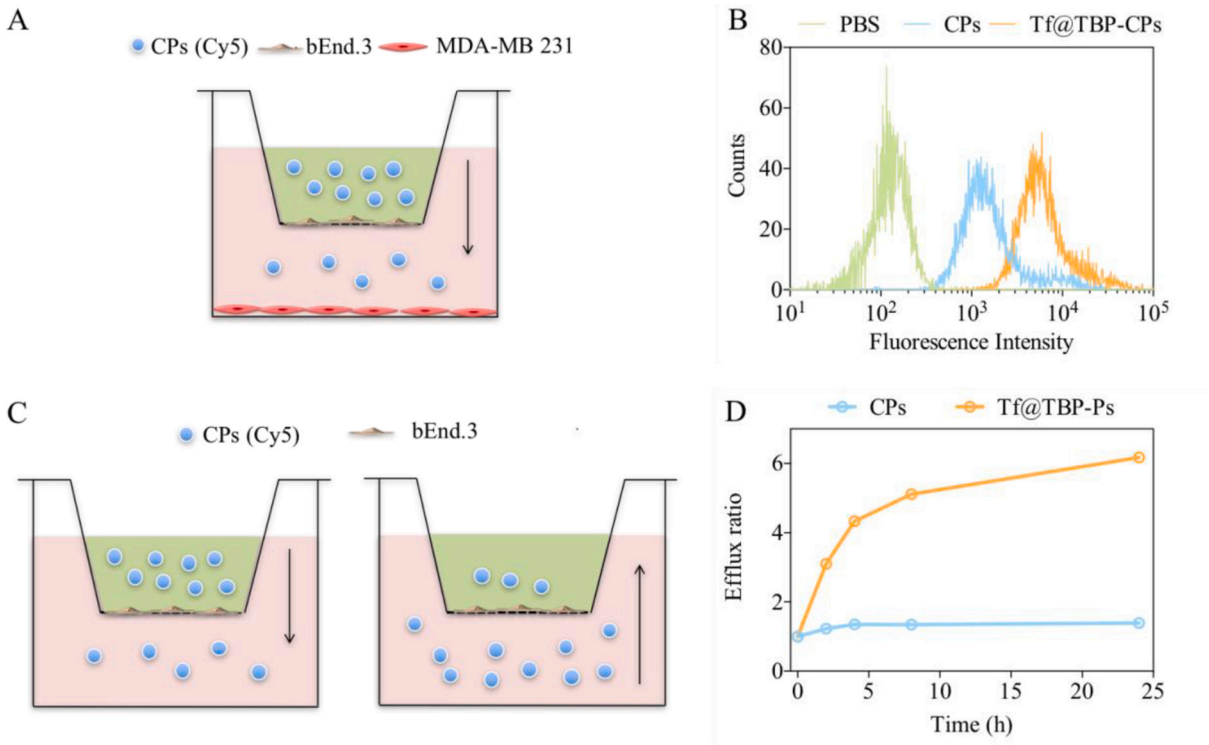

Fig. 2. (A) Schematic illustration of bEnd.3 monolayer seeded in the upper chamber and MDA-MB 231 cell monolayer in the lower chamber. (B) The uptake of CPs (Cy5) and Tf@TBP-CPs (Cy5) in MDA-MB 231 cells in the lower chamber measured using flow cytometry. (C) Schematic illustration of efflux ratio assays. (D) The efflux ratios of CPs (Cy5) and Tf@TBP-CPs (Cy5) over time.

TfR overexpressed cells. The internalization of Tf@TBP-CPs-siPLK1 (Cy5) by the cells was greatly repressed at 4 °C or in the presence of the ATP inhibitor sodium azide (Fig. 1G), indicating that Tf@TBP-CPs-siPLK1(Cy5) is internalized by MDA-MB 231 cells *via* energy-dependent endocytosis process. The internalization pathway of Tf@TBP-CPs-siPLK1(Cy5) was further investigated by treating MDA-MB 231 cells with various endocytic inhibitors such as amiloride hydrochloride, chlorpromazine (CPZ), or methyl-β-cyclodextrins (MβCD). Fig. 1H displays that the internalization of Tf@TBP-CPs-siPLK1(Cy5) was markedly obstructed by treatment of CPZ, amiloride hydrochloride, and MβCD, indicating that the cellular internalization of Tf@TBP-CPs-siPLK1(Cy5) is mediated not only by clatherin/dynamin but also by caveolae-mediated and macropinocytosis pathways. This result is interesting and different from a previous report that clathrin/dynamin-mediated endocytosis dominates Tf/TfR complex internalization [42].

3.3. *In vitro BBB permeation*

The bEnd.3 (immortalized mouse brain endothelial cell line) monolayers and MDA-MB 231 cells were co-cultured to study BBB passage and subsequent breast cancer cell targeting of Cy5-labeled Tf@TBP-CPs. TfR has been reported to highly express on bEnd.3 endothelial cells and on MDA-MB 231 cells [43,44]. As shown in Fig. 2A, the bEnd.3 was seeded as monolayer on the bottom of the upper chamber (TEER over 200 $\Omega \cdot cm^2$) to simulate the BBB, and MDA-MB 231 cells were seeded as monolayer on the bottom of the lower chamber. The *in vitro* BBB monolayers were complete after 2 days culturing of bEnd.3 cells and remained intact until the end of the experiment as confirmed by TEER value. The results showed 5-fold enhanced association of Tf@TBP-CPs (Cy5) with MDA-MB 231 cells compared with non-targeted CPs(Cy5) (Fig. 2B), signifying that Tf@TBP-CPs(Cy5) mediate more effective BBB transcytosis and contact with MDA-MB 231 cells. We further carried out the efflux ratio assays for Tf@TBP-CPs(Cy5) to eradicate the non-specific paracellular permeability of the monolayer (Fig. 2C). The results revealed that CPs(Cy5) had efflux ratios close to 1.4 in 24 h whereas the efflux ratio of Tf@TBP-CPs(Cy5) increased to 6.2 (Fig. 2D). The angiopep-2 decorated polymersomes were found an efflux ratio of 2.5 after 24 h incubation [45]. These results confirmed that Tf bounded chimeric polymersomes revealed excellent and selective BBB permeability.

3.4. *TfR-mediated siRNA delivery and gene silencing in vitro*

The targetability and intracellular siRNA delivery capability of Tf@TBP-CPs and control CPs were studied by CSLM using siPLK1(Cy3) as a model siRNA in MDA-MB 231 cells by CLSM. The CLSM images of cells after 12 h incubation revealed much stronger intracellular Cy3 fluorescence for Tf@TBP-CPs-siPLK1(Cy3) compared with CPs-siPLK1 (Cy3) (Fig. 3A). The *in vitro* gene silencing experiments performed using siRNA against EGFP (siEGFP) in MDA-MB 231-EGFP cells displayed that the EGFP expression was markedly inhibited by Tf@TBP-CPs-siEGFP while CPs-siEGFP caused little inhibition of EGFP expression (Fig. 3B). Quantitative fluorescence analysis indicated a strong ligand-mediated gene silencing. Tf@TBP-CPs-siEGFP revealed about 75% fluorescence reduction at 100 nM, in comparison to about 25% for the control CPs-siEGFP (Fig. 3C). The qPCR analyses showed that in contrast to Tf@TBP-CPs-siScramble, Tf@TBP-CPs-siPLK1 brought about significant siPLK1 silencing in MDA-MB 231 cells (Fig. S1), supporting the specificity of siPLK1.

The MTT assays were utilized to evaluate the cytotoxicity of Tf@TBP-CPs-siPLK1 and Tf@TBP-CPs-siScramble towards EGFP-overexpressing MDA-MB 231 cells. As anticipated, no obvious cytotoxicity was found for both CPs-siScramble and Tf@TBP-CPs-siScramble (Fig. 3D). However, in case of Tf@TBP-CPs-siPLK1, significantly higher cell death was observed at 100 nM compared with CPs-siPLK1 (Fig. 3E), confirming the targeted silencing effect of Tf@TBP-CPs-siPLK1. The reason that Tf@TBP-CPs caused only moderate reduction of cell viability is that unlike cytotoxic drugs that directly kill cancer

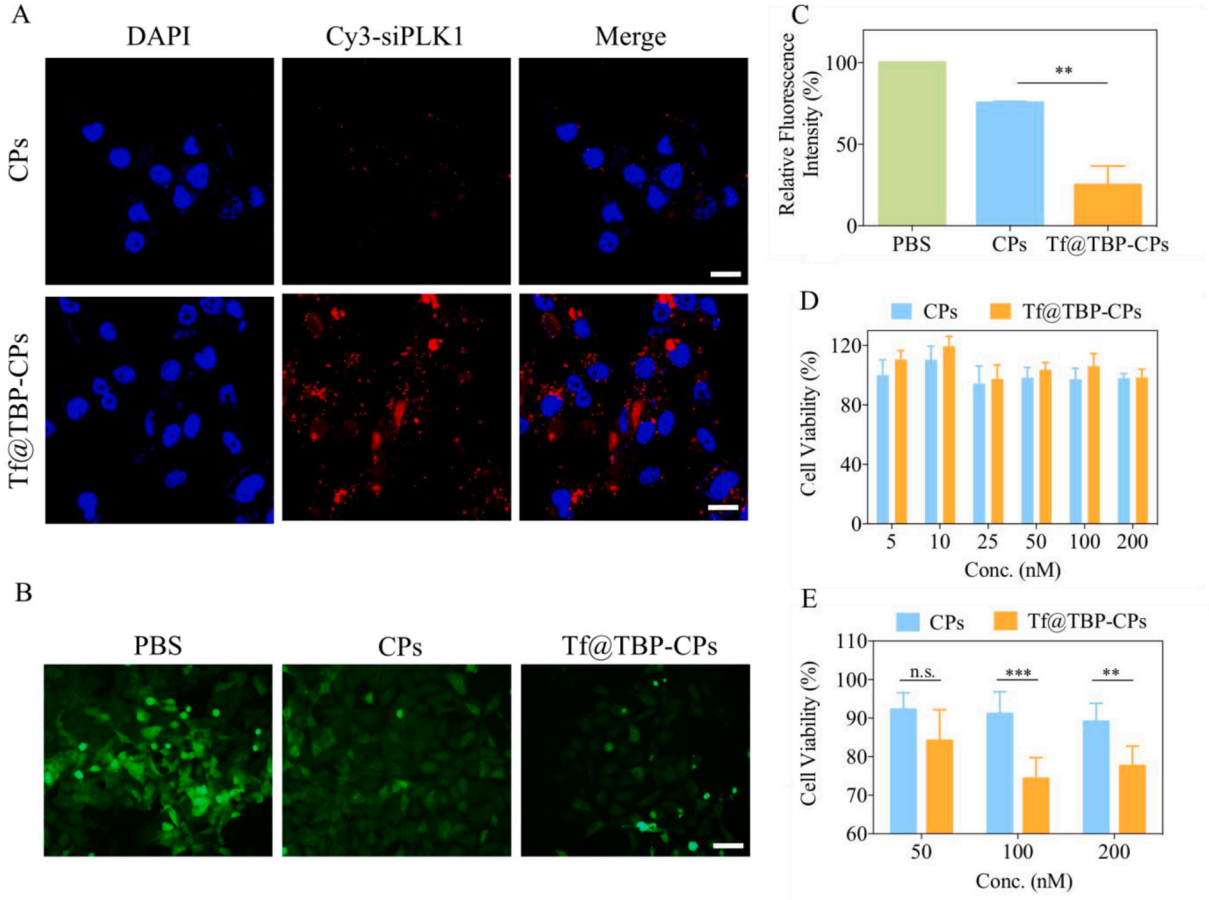

Fig. 3. (A) Intracellular siPLK1(Cy3) release from Tf@TBP-CPs-siPLK1(Cy3) and CPs-siPLK1(Cy3) observed by CLSM after 12 h incubation. Scale Bar: 25 μm. (B) *In vitro* silencing of EGFP expression in MDA-MB 231-EGFP cells with siEGFP-loaded CPs or Tf@TBP-CPs (Dosage: 100 nM). The cells incubated for 12 h with siEGFP-loaded CPs or Tf@TBP-CPs were thereafter cultured for another 36 h. Scale Bar: 50 μm. (C) Semi-quantitative fluorescence analysis by software Image J after siEGFP treatment. (D) Viability of MDA-MB 231 cells after treating with siScramble-loaded CPs or siScramble-loaded Tf@TBP-CPs. The data are presented as mean ± SD (n = 6). (E) Viability of MDA-MB 231 cells after treating with 50, 100 or 200 nM CPs-siPLK1 or Tf@TBP-CPs-siPLK1, The data are presented as mean ± SD (n = 6).

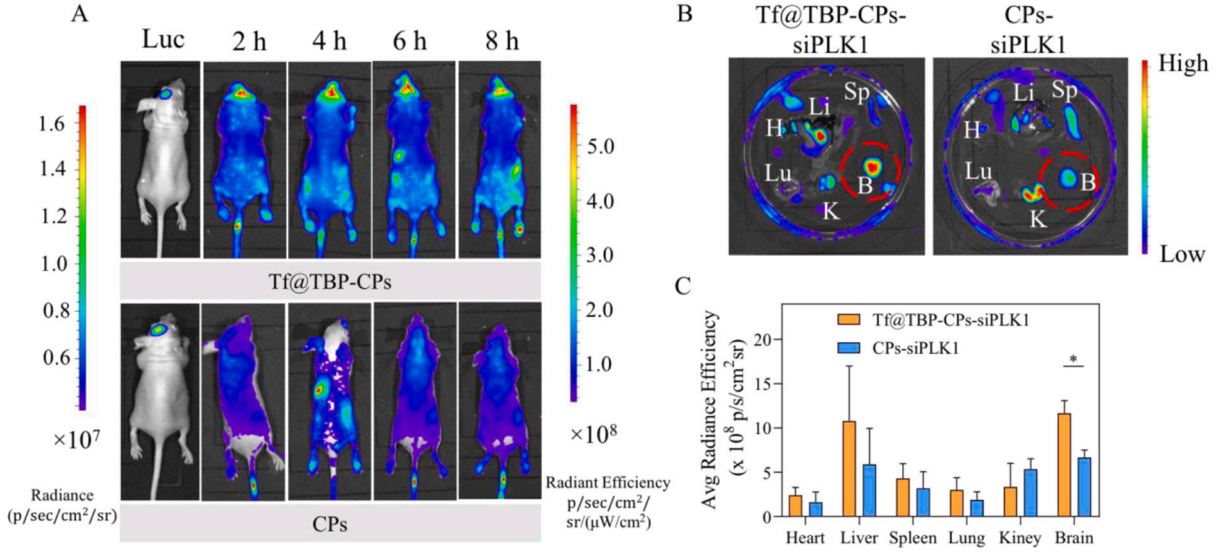

Fig. 4. (A) NIR images of the mice bearing intracranial MDA-MB 231-Luc tumor brain metastases at 2, 4, 6 and 8 h post injection of Tf@TBP-CPs-siPLK1(Cy5) or CPs-siPLK1(Cy5). Luc indicated the tumor bioluminescence at 0 h. (B) The *ex vivo* imaging and (C) fluorescence semi-quantification of excised major organs and tumors at 8 h after injection of Tf@TBP-CPs-siPLK1(Cy5) or CPs-siPLK1(Cy5). siPLK1(Cy5) dosage: 0.5 mg/kg.

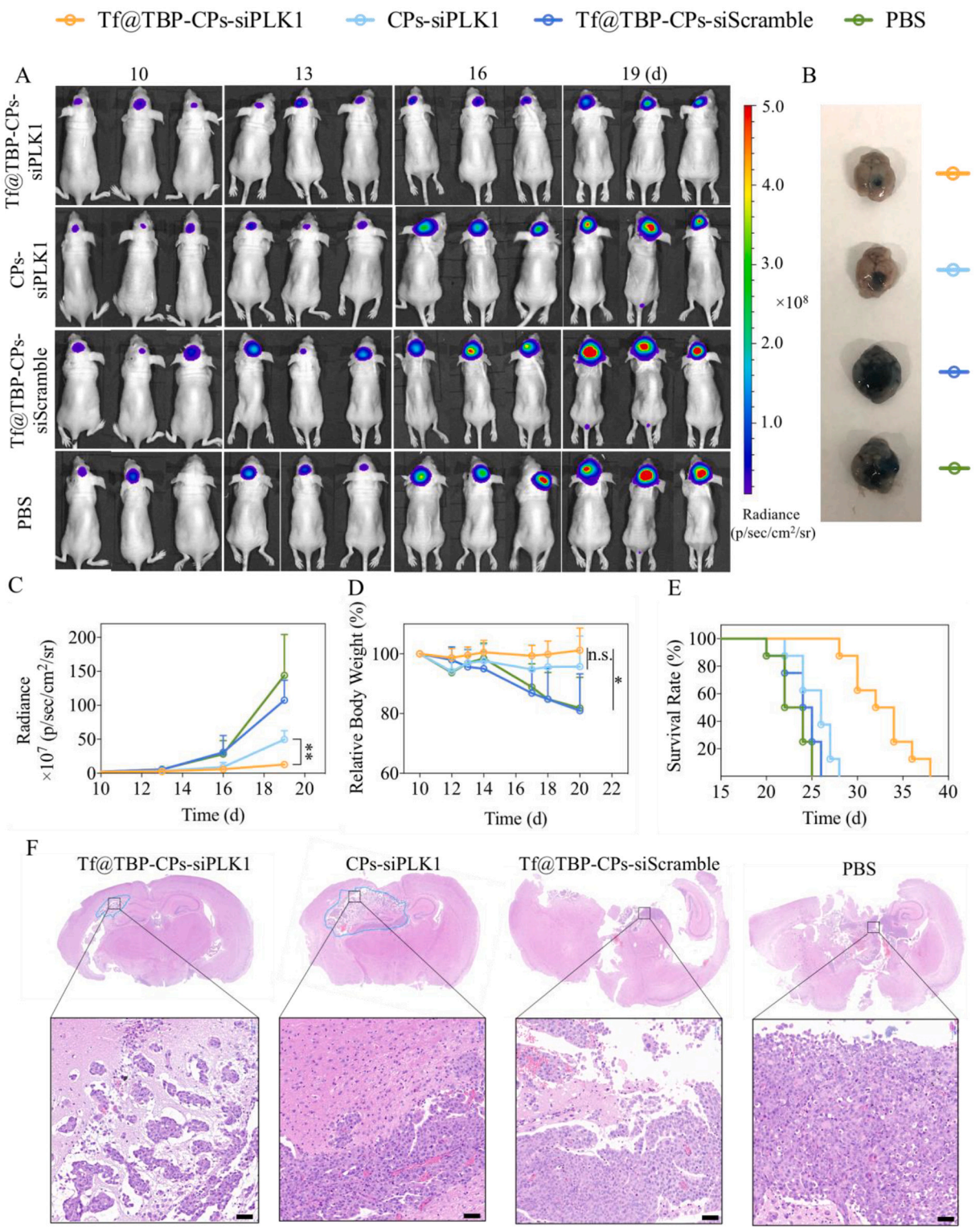

Fig. 5. *In vivo* anti-brain metastases efficacy of Tf@TBP-CPs-siPLK1 (dosage: 2 mg/kg) in intracranial MDA-MB 231 breast cancer bearing mice ($n = 8$). siScramble was used as a negative control. (A) Bioluminescence images of mice on day 10, 13, 16 and 19. (B) The photograph of excised brain with Evans Blue staining. (C) Semi-quantitative analysis of mean bioluminescence intensity of MDA-MB 231-Luc in the brain. (D) Body weight changes of mice within 20 days. (E) Survival curves. Kaplan-Meier analysis: Tf@TBP-CPs-siPLK1 *vs* PBS, CPs-siPLK1, or Tf@TBP-CPs-siScramble: ***$p < 0.001$; CPs-siPLK1 *vs* PBS: *$p < 0.05$. (F) The whole brain scan using H&E staining (Scar bars: 50 μm). (For interpretation of the references to colour in this figure legend, the reader is referred to the web version of this article.)

cells siPLK1 causes inhibitory effect by arresting the cell cycle in G2/M phase [46,47].

3.5. *In vivo* pharmacokinetics and brain metastases targeting

The accumulation of Tf@TBP-CPs-siPLK1(Cy5) in an intracranial MDA-MB 231-Luc brain metastases model was tracked using *in vivo* NIR

imaging system. Notably, Cy5 fluorescence was observed at the intracranial breast tumor at 2 h post-injection of Tf@TBP-CPs-siPLK1(Cy5) and kept strong at 8 h post-injection (Fig. 4A). Only weak Cy5 fluorescence was detected in the tumor for CPs-siPLK1(Cy5) throughout the entire 8 h period. The *ex-vivo* imaging verified much higher Cy5 fluorescence intensity in intracranial breast tumor for Tf@TBP-CPs-siPLK1 (Cy5) than for the non-targeted counterpart (Fig. 4B,C), supporting that Tf@TBP-CPs-siPLK1(Cy5) selectively accumulates in the tumor lesion. The accumulation of CPs-siPLK1(Cy5) in brain metastases was ascribed to the EPR effect, which was reported to increases along with the progression of tumor [48]. Moreover, Tf@TBP-CPs-siPLK1(Cy5) gave less spleen and kidney accumulation than CPs-siPLK1(Cy5), which is possibly related to Tf coating that not only reduces protein corona formation but also prevents siRNA leakage. Notably, Tf@TBP-CPs-siPLK1(Cy5) showed also enhanced accumulation in the liver, which could be ascribed to the expression of TfR in the liver [49].

3.6. Treatment of intracranial MDA-MB 231-Luc tumor

The anti-brain metastases activity of Tf@TBP-CPs-siPLK1 was examined using an intracranial MDA-MB 231-Luc tumor xenografts at 2 mg siPLK1/kg. The *in vivo* bioluminescence images indicated that Tf@TBP-CPs-siPLK1 significantly retarded the tumor progression compared with the non-targeted CPs-siPLK1 and Tf@TBP-CPs-sicramble groups (Fig. 5A). At day 20, one mouse was sacrificed from each group and the tumor was stained with Evans blue by perfusion prior to sacrifice. The photos of stained tumors corroborated effective tumor inhibition by Tf@TBP-CPs-siPLK1 (Fig. 5B). On the contrary, tumor invaded into the whole brain for the control Tf@TBP-CPs-siScramble and PBS treatments. Fig. 5C shows clearly that the tumor bioluminescence in the Tf@TBP-CPs-siPLK1 treatment group was significantly weaker than that in CPs-siPLK1, Tf@TBP-CPs-siScramble and PBS groups. In accordance, the body weight of mice after PBS or Tf@TBP-CPs-siScramble treatment dropped rapidly owing to massive tumor invasion and brain disorder. No body weight loss was observed for the Tf@TBP-CPs-siPLK1 treated group, suggesting that effective treatment with Tf@TBP-CPs-siPLK1 leading to retardation of tumor invasion can be realized without inducing unacceptable side effects (Fig. 5D).

Kaplan-Meier survival curves disclosed that Tf@TBP-CPs-siPLK1 considerably prolonged the median survival time of the mice compared with CPs-siPLK1, Tf@TBP-CPs-siScramble and PBS (33 *versus* 26, 24 and 23 days, respectively) (Fig. 5E). The H&E staining of the brains confirmed that the animals in the Tf@TBP-CPs-siPLK1 treatment group showed the smallest brain tumor area among all groups (Fig. 5F). Furthermore, no noticeable tissue damage was observed in the H&E staining images of heart, liver, spleen, lung and kidney, signifying the good safety of Tf@TBP-CPs-siPLK1 (Fig. S2). Notably, CPs are based on PEG, trimethylene carbonate copolymer, and spermine, which are mostly safe materials. The above data strongly suggest that Tf@TBP-CPs-siPLK1 is capable of penetrating the BBB and brings about efficient and targeted gene therapy of breast tumor brain metastases *in vivo*.

4. Conclusion

Transferrin-functionalized polymersomal siPLK1 (Tf@TBP-CPs-siPLK1) has been developed to pass the BBB and elicit specific gene silencing in breast cancer brain metastatic cells, yielding effective inhibition of tumor growth and significant improvement of survival time. Moreover, Tf@TBP-CPs-siPLK1 shows no apparent systemic toxicity, as reflected by the absence of body weight loss during the treatment period and histological analysis. The surface-bound transferrin facilitates BBB transcytosis and subsequently specifically directs polymersomal siPLK1 to intracranial MDA-MB 231 breast tumor cells. This transferrin binding strategy is robust and is based on novel and facile production of transferrin-targeted siRNA nanoformulations *via* the use of preformed TBP-exposing CPs, avoiding sophisticated chemical procedures to couple Tf and additionally the risk of Tf interfering with siRNA encapsulation. This selective transferrin coating appears to be a particularly facile strategy to fabricate BBB-permeable and targeted vesicles for potent RNAi therapy of breast cancer brain metastases.

Credit author statement

Y. H. Wei and Y. P. Sun carried out the experiments and drafted the paper; J. J. Wei and X. Y. Qiu synthesized and investigated the co-polymers; F. H. Meng, G. Storm, and Z. Y. Zhong co-supervised the work and revised the paper.

Acknowledgements

This work is supported by the National Natural Science Foundation of China (51633005, 51861145310). JJ Wei thanks the support from Post Graduate Research & Practice Innovation Program of Jiangsu Province (KYCX19 1901).

Appendix A. Supplementary data

Supplementary data to this article can be found online at https://doi.org/10.1016/j.jconrel.2021.07.048.

References

[1] J.S. Barnholtz-Sloan, A.E. Sloan, F.G. Davis, F.D. Vigneau, P. Lai, R.E. Sawaya, Incidence proportions of brain metastases in patients diagnosed (1973 to 2001) in the metropolitan Detroit cancer surveillance system, J. Clin. Oncol. 22 (2004) 2865–2872.

[2] P.W. Sperduto, S.T. Chao, P.K. Sneed, X.H. Luo, J. Suh, D. Roberge, A. Bhatt, A. W. Jensen, P.D. Brown, H. Shih, J. Kirkpatrick, A. Schwer, L.E. Gaspar, J. B. Fiveash, V. Chiang, J. Knisely, C.M. Sperduto, M. Mehta, Diagnosis-specific prognostic factors, indexes, and treatment outcomes for patients with newly diagnosed brain metastases: a multi-institutional analysis of 4,259 patients, Int. J. Radiat. Oncol. 77 (2010) 655–661.

[3] A.S. Berghoff, S. Schur, L.M. Fureder, B. Gatterbauer, K. Dieckmann, G. Widhalm, J. Hainfellner, C.C. Zielinski, P. Birner, R. Bartsch, M. Preusser, Descriptive statistical analysis of a real life cohort of 2419 patients with brain metastases of solid cancers, Esmo Open 1 (2016).

[4] H. Nitta, B.D. Kelly, C. Allred, S. Jewell, P. Banks, E. Dennis, T.M. Grogan, The assessment of HER2 status in breast cancer: the past, the present, and the future, Pathol. Int. 66 (2016) 313–324.

[5] T. Bachelot, G. Romieu, M. Campone, V. Dieras, C. Cropet, F. Dalenc, M. Jimenez, E. Le Rhun, J.Y. Pierga, A. Goncalves, M. Leheurteur, J. Domont, M. Gutierrez, H. Cure, J.M. Ferrero, C. Labbe-Devilliers, Lapatinib plus capecitabine in patients with previously untreated brain metastases from HER2-positive metastatic breast cancer (LANDSCAPE): a single-group phase 2 study, Lancet Oncol. 14 (2013) 64–71.

[6] A.M. Hamilton, S. Aidoudi-Ahmed, S. Sharma, V.R. Kotamraju, P.J. Foster, K. N. Sugahara, E. Ruoslahti, B.K. Rutt, Nanoparticles coated with the tumor-penetrating peptide iRGD reduce experimental breast cancer metastasis in the brain, J. Mol. Med. 93 (2015) 991–1001.

[7] A. Thulin, E. Rönnerman, C. Zhang, S. De Lara, C. Chamalidou, A. Schoenfeldt, C. Andersson, A. Kovács, F. Enlund, B. Linderholm, Clinical outcome of patients with brain metastases from breast cancer-a population based study over 21 years, Breast 50 (2020) 113–124.

[8] A.S. Mohammad, J.I. Griffith, C.E. Adkins, N. Shah, E. Sechrest, E.L. Dolan, T. B. Terrell-Hall, B.S. Hendriks, H. Lee, P.R. Lockman, Liposomal irinotecan cccumulates in metastatic lesions, crosses the blood-tumor barrier (BTB), and prolongs survival in an experimental model of brain metastases of triple negative breast cancer, Pharm. Res. 35 (2018).

[9] M. Li, K.R. Shi, X. Tang, J.J. Wei, X.L. Cun, Y. Long, Z.R. Zhang, Q. He, Synergistic tumor microenvironment targeting and blood-brain barrier penetration via a pH-responsive dual-ligand strategy for enhanced breast cancer and brain metastasis therapy, Nanomed-Nanotechnol. 14 (2018) 1833–1843.

[10] C.D. Arvanitis, V. Askoxylakis, Y. Guo, M. Datta, J. Kloepper, G.B. Ferraro, M. O. Bernabeu, D. Fukumura, N. McDannold, R.K. Jain, Mechanisms of enhanced drug delivery in brain metastases with focused ultrasound-induced blood–tumor barrier disruption, P. Natl. Acad. Sci. USA 115 (2018) 8717–8726.

[11] C.S. He, J.S. Li, P. Cai, T. Ahmed, J.T. Henderson, W.D. Foltz, R. Bendayan, A. M. Rauth, X.Y. Wu, Two-step targeted hybrid nanoconstructs increase brain penetration and efficacy of the therapeutic antibody trastuzumab against brain metastasis of HER2-positive breast cancer, Adv. Funct. Mater. 28 (2018).

[12] Q. Guo, Q.N. Zhu, T.T. Miao, J. Tao, X.F. Ju, Z.L. Sun, H. Li, G.Q. Xu, H.B. Chen, L. Han, LRP1-upregulated nanoparticles for efficiently conquering the blood-brain barrier and targetedly suppressing multifocal and infiltrative brain metastases, J. Control. Release 303 (2019) 117–129.

[13] C.S. He, P. Cai, J. Li, T. Zhang, L. Lin, A.Z. Abbasi, J.T. Henderson, A.M. Rauth, X. Y. Wu, Blood-brain barrier-penetrating amphiphilic polymer nanoparticles deliver docetaxel for the treatment of brain metastases of triple negative breast cancer, J. Control. Release 246 (2017) 98–109.
[14] R.A. Morshed, M.E. Muroski, Q. Dai, M.L. Wegscheid, B. Auffinger, D. Yu, Y. Han, L.J. Zhang, M.J. Wu, Y. Cheng, M.S. Lesniak, Cell-penetrating peptide-modified gold nanoparticles for the delivery of doxorubicin to brain metastatic breast cancer, Mol. Pharma. 13 (2016) 1843–1854.
[15] I. Zafir-Lavie, S. Sherbo, H. Goltsman, F. Badinter, E. Yeini, P. Ofek, R. Miari, O. Tal, A. Liran, T. Shatil, S. Krispel, N. Shapir, G.A. Neil, I. Benhar, A. Panet, R. Satchi-Fainaro, Successful intracranial delivery of trastuzumab by gene-therapy for treatment of HER2-positive breast cancer brain metastases, J. Control. Release 291 (2018) 80–89.
[16] W. Gu, F. Meng, R. Haag, Z. Zhong, Actively targeted nanomedicines for precision cancer therapy: concept, construction, challenges and clinical translation, J. Control. Release 329 (2021) 676–695.
[17] D. Bumcrot, M. Manoharan, V. Koteliansky, D.W.Y. Sah, RNAi therapeutics: a potential new class of pharmaceutical drugs, Nat. Chem. Biol. 2 (2006) 711–719.
[18] Y. Zhang, A. Satterlee, L. Huang, In vivo gene delivery by nonviral vectors: overcoming hurdles? Mol. Ther. 20 (2012) 1298–1304.
[19] M.R. Lares, J.J. Rossi, D.L. Ouellet, RNAi and small interfering RNAs in human disease therapeutic applications, Trends Biotechnol. 28 (2010) 570–579.
[20] K. Strebhardt, A. Ullrich, Opinion-targeting polo-like kinase 1 for cancer therapy, Nat. Rev. Cancer 6 (2006) 321–330.
[21] S. Dou, X.Z. Yang, M.H. Xiong, C.Y. Sun, Y.D. Yao, Y.H. Zhu, J. Wang, ScFv-decorated PEG-PLA-based nanoparticles for enhanced siRNA delivery to Her2(+) breast cancer, Adv. Healthc. Mater. 3 (2014) 1792–1803.
[22] Y. Zou, M. Zheng, W.J. Yang, F.H. Meng, K. Miyata, H.J. Kim, K. Kataoka, Z. Y. Zhong, Virus-mimicking chimaeric polymersomes boost targeted cancer siRNA therapy in vivo, Adv. Mater. 29 (2017).
[23] G. Ozcan, B. Ozpolat, R.L. Coleman, A.K. Sood, G. Lopez-Berestein, Preclinical and clinical development of siRNA-based therapeutics, Adv. Drug Deliv. Rev. 87 (2015) 108–119.
[24] S.J. Tan, P. Kiatwuthinon, Y.H. Roh, J.S. Kahn, D. Luo, Engineering nanocarriers for siRNA delivery, Small 7 (2011) 841–856.
[25] R. Kanasty, J.R. Dorkin, A. Vegas, D. Anderson, Delivery materials for siRNA therapeutics, Nat. Mater. 12 (2013) 967–977.
[26] W.M. Pardridge, Delivery of biologics across the blood-brain barrier with molecular trojan horse technology, Biodrugs 31 (2017) 503–519.
[27] Y. Uchida, S. Ohtsuki, Y. Katsukura, C. Ikeda, T. Suzuki, J. Kamiie, T. Terasaki, Quantitative targeted absolute proteomics of human blood-brain barrier transporters and receptors, J. Neurochem. 117 (2011) 333–345.
[28] E.A. Wyatt, M.E. Davis, Method of establishing breast cancer brain metastases affects brain uptake and efficacy of targeted, therapeutic nanoparticles, Bioeng. Transl. Med. 4 (2019) 30–37.
[29] G. Hultqvist, S. Syvanen, X.T. Fang, L. Lannfelt, D. Sehlin, Bivalent brain shuttle increases antibody uptake by monovalent binding to the transferrin receptor, Theranostics 7 (2017) 308–318.
[30] X.N. Song, R. Li, H.L. Deng, Y. Li, Y.N. Cui, H. Zhang, W.B. Dai, B. He, Y. Zheng, X. Q. Wang, Q. Zhang, Receptor mediated transcytosis in biological barrier: the influence of receptor character and their ligand density on the transmembrane pathway of active-targeting nanocarriers, Biomaterials 180 (2018) 78–90.
[31] S. Ayloo, C.H. Gu, Transcytosis at the blood-brain barrier, Curr. Opin. Neurobiol. 57 (2019) 32–38.
[32] D. Yang, D.C. Liu, H.L. Deng, J. Zhang, M.M. Qin, L. Yuan, X.J. Zou, B. Shao, H. P. Li, W.B. Dai, H. Zhang, X.Q. Wang, B. He, X. Tang, Q. Zhang, Transferrin functionization elevates transcytosis of nanogranules across epithelium by triggering polarity-associated transport flow and positive cellular feedback loop, ACS Nano 13 (2019) 5058–5076.
[33] A. Jhaveri, P. Deshpande, B. Pattni, V. Torchilin, Transferrin-targeted, resveratrol-loaded liposomes for the treatment of glioblastoma, J. Control. Release 277 (2018) 89–101.
[34] Y.F. Li, M. Chen, B.W. Yao, X. Lu, X.Q. Zhang, P. He, S.N. Vasilatos, X.M. Ren, W. H. Bian, C. Yao, Transferrin receptor-targeted redox/pH-sensitive podophyllotoxin prodrug micelles for multidrug-resistant breast cancer therapy, J. Mater. Chem. B 7 (2019) 5814–5824.
[35] J.Y. Yhee, S.J. Lee, S. Lee, S. Song, H.S. Min, S.W. Kang, S. Son, S.Y. Jeong, I. C. Kwon, S.H. Kim, K. Kim, Tumor-targeting transferrin nanoparticles for systemic polymerized siRNA delivery in tumor-bearing mice, Bioconjug. Chem. 24 (2013) 1850–1860.
[36] W. Zhang, K. Muller, E. Kessel, S. Reinhard, D.S. He, P.M. Klein, M. Hohn, W. Rodl, S. Kempter, E. Wagner, Targeted siRNA delivery using a lipo-oligoaminoamide nanocore with an influenza peptide and transferrin shell, Adv. Healthc. Mater. 5 (2016) 1493–1504.
[37] A. Kohata, P.K. Hashim, K. Okuro, T. Aida, Transferrin-appended nanocaplet for transcellular siRNA delivery into deep tissues, J. Am. Chem. Soc. 141 (2019) 2862–2866.
[38] M. Santi, G. Maccari, P. Mereghetti, V. Voliani, S. Rocchiccioli, N. Ucciferri, S. Luin, G. Signore, Rational design of a transferrin-binding peptide sequence tailored to targeted nanoparticle internalization, Bioconjug. Chem. 28 (2017) 471–480.
[39] Y. Wei, X. Gu, Y. Sun, F. Meng, G. Storm, Z. Zhong, Transferrin-binding peptide functionalized polymersomes mediate targeted doxorubicin delivery to colorectal cancer in vivo, J. Control. Release 319 (2020) 407–415.
[40] P.L. Yao, Y.F. Zhang, H. Meng, H.L. Sun, Z.Y. Zhong, Smart polymersomes dually functionalized with cRGD and fusogenic GALA peptides enable specific and high-efficiency cytosolic delivery of apoptotic proteins, Biomacromolecules 20 (2019) 184–191.
[41] Y. Zhong, F. Meng, W. Zhang, B. Li, J.C. van Hest, Z. Zhong, CD44-targeted vesicles encapsulating granzyme B as artificial killer cells for potent inhibition of human multiple myeloma in mice, J. Control. Release 320 (2020) 421–430.
[42] S. Tortorella, T.C. Karagiannis, Transferrin ceceptor-mediated endocytosis: a useful target for cancer therapy, J. Membrane Biol. 247 (2014) 291–307.
[43] M.S. Muthu, R.V. Kutty, Z.T. Luo, J.P. Xie, S.S. Feng, Theranostic vitamin E TPGS micelles of transferrin conjugation for targeted co-delivery of docetaxel and ultra bright gold nanoclusters, Biomaterials 39 (2015) 234–248.
[44] J. Zhou, M.H. Li, W.Q. Lim, Z. Luo, S.Z.F. Phua, R.L. Huo, L.Q. Li, K. Li, L.L. Dai, J. J. Liu, K.Y. Cai, Y.L. Zhao, A transferrin-conjugated hollow nanoplatform for redox-controlled and targeted chemotherapy of tumor with reduced inflammatory reactions, Theranostics 8 (2018) 518–532.
[45] Y.N. Shi, Y. Jiang, J.S. Cao, W.J. Yang, J. Zhang, F.H. Meng, Z.Y. Zhong, Boosting RNAi therapy for orthotopic glioblastoma with nontoxic brain-targeting chimaeric polymersomes, J. Control. Release 292 (2018) 163–171.
[46] X. Liu, R.L. Erikson, Polo-like kinase (Plk) 1 depletion induces apoptosis in cancer cells, P. Natl. Acad. Sci. USA 100 (2003) 5789–5794.
[47] M. Reda, W. Ngamcherdtrakul, S. Gu, D.S. Bejan, N. Siriwon, J.W. Gray, W. Yantasee, PLK1 and EGFR targeted nanoparticle as a radiation sensitizer for non-small cell lung cancer, Cancer Lett. 467 (2019) 9–18.
[48] Y. Jiang, W.J. Yang, J. Zhang, F.H. Meng, Z.Y. Zhong, Protein toxin chaperoned by LRP-1-targeted virus-mimicking vesicles induces high-efficiency glioblastoma therapy in vivo, Adv. Mater. 30 (2018).
[49] Y. Liu, H.-Y. Wang, L. Zhou, Y. Su, W.-C. Shen, Biodistribution, activation, and retention of proinsulin-transferrin fusion protein in the liver: mechanism of liver-targeting as an insulin prodrug, J. Control. Release 275 (2018) 186–191.